Chemical Science

ROYAL SOCIETY OF CHEMISTRY

EDGE ARTICLE

View Article Online
View Journal

Cite this: DOI: 10.1039/d5sc09502f

All publication charges for this article have been paid for by the Royal Society of Chemistry

Chemical recycling of imine-linked covalent organic frameworks

Yimiao Jing, Jie Wang, Yu Fang and Zhongshan Liu *

Imine-linked covalent organic frameworks (COFs) have been explored for various applications; however, chemical recycling of end-of-life COFs is an undeveloped area of research. Here, we report closed-loop recycling methods for imine-linked COFs, realizing their chemical depolymerization and reconstruction through dynamic imine chemistry. An alkyl monoamine with a stronger nucleophilicity is adopted to attack aromatic imine linkages of COFs at room temperature, depolymerizing the crosslinked frameworks into small molecular alkyl-imines and aromatic amine monomers. To accelerate depolymerization rates, we further combine the monoamine with $Sc(OTf)_3$ to shorten depolymerization time by a factor of 8. The alkyl-substituted imines are unstable in the presence of acetic acid and easily revert back to the aromatic imines *via* reversible transamination, enabling *in situ* regeneration of COFs without tedious monomer purification and with recoveries up to 92%. As evidenced by powder X-ray diffraction and nitrogen and benzene vapor adsorption measurements, the recovered COFs retain their crystallinity, characteristic pore size and adsorption performance. The successful recycling of imine-linked COFs offers a promising strategy for the sustainable development of porous organic materials.

Received 4th December 2025
Accepted 11th February 2026

DOI: 10.1039/d5sc09502f

rsc.li/chemical-science

Introduction

Covalent organic frameworks (COFs), featuring customizable topologies and permanent porosities,[1] have demonstrated potential applications in adsorption,[2–5] separation,[6–8] catalysis,[9–11] and sensing.[12–15] Despite their functional superiority, the high cost of building blocks is one of the limitations for COF production on a large scale and their commercial applications. Especially for imine-linked COFs, end-of-life materials may release toxic compounds, such as anilines that can serve as precursors of disinfection byproducts in water.[16] Unlike booming synthetic methods and applications, the chemical recycling of end-of-life COFs remains undeveloped. But this should be of significance for environmental and economic sustainability and for practical applications of COF materials. Several studies have attempted physical recovery strategies by means of adsorption–desorption or magnetic separation.[17–19] However, these methods struggle to retain the structural integrity and performance stability of the recovered COFs and also fail to recycle physically inseparable COF moieties from composite materials. Therefore, developing a chemical recycling strategy that can regenerate high-quality COFs is highly desired.

Dynamic imine chemistry, which is classified as reversible imine condensation, transimination and imine metathesis, has evolved from the study of small molecular reaction mechanisms to the synthesis of functional supermolecules and polymers.[20–25] Typically, reactions of aldehydes with amines generate imine compounds that can also revert back to starting monomers (Fig. 1a). This reversibility between imine condensation and hydrolysis enables polymeric network self-correction under suitable conditions and formation of crystalline imine-linked COFs.[26] Compared to imine condensation, transamination based on amine–imine exchange shows a controllable reaction process, which has emerged as a versatile tool to produce single-crystal COFs.[27,28]

Most imine-linked COFs are made with aromatic amines because rigid conjugated networks contribute to framework formation and good stability. However, aromatic amines have an inferior nucleophilicity compared to alkylamines. This difference would drive the hydrolysis of aromatic imines and formation of alkyl-substituted imines (Fig. 1a). Paradoxically, preferentially formed alkyl-imines possess relatively poorer stability than conjugated aromatic imines, especially under acidic conditions. Inspired by such transimination, here we present a closed-loop recycling method for imine-linked COFs, including two steps of chemical depolymerization and regeneration. An alkyl monoamine is used as a nucleophilic agent to depolymerize imine-linked frameworks into small molecular alkyl-imines and aromatic amine monomers. Then we leverage the instability of alkyl-imines to regenerate crystalline COFs in the presence of acetic acid.

Although the transimination reactions of small molecules in dilute solutions were well studied using the NMR

MOE Key Laboratory of Applied Surface and Colloid Chemistry, School of Chemistry and Chemical Engineering, Shaanxi Normal University, Xi'an, 710119, China. E-mail: zhongshan.liu@snnu.edu.cn

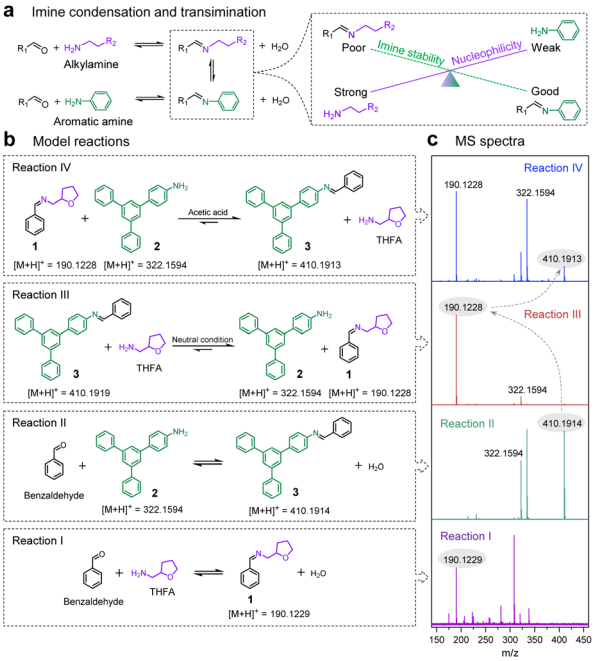

Fig. 1 (a) Schematic illustrations for imine condensation and transimination. (b) Model reactions of imine condensation (Reactions I and II) and reversible transimination (Reactions III and IV). (c) MS spectra of model reaction mixtures (raw data, see also Fig. S60–S63). Corresponding chromatograms can be seen in Fig. S1.

technique,[23,29–31] the path toward the solid COF recovery poses several challenges: (i) unlike model reactions with small molecules, the heterogeneous depolymerization of crosslinked COFs involves a complex dynamic process, but it is poorly understood. (ii) The amount of monoamine that is required for complete depolymerization of solid COFs is uncertain. (iii) The kinetic limitations between liquid reagents and solid COFs take more time. (iv) Reverting back to aromatic imine-linked amorphous polymers may easily occur, but reconstruction of original properties of COFs is difficult. For instance, their crystallinity and porosity are two necessary criteria to define frameworks. To tackle these problems, we need to optimize the ratios of monoamine to COFs and use an NMR instrument and a mass spectrometer (MS) to identify the depolymerization products. After building depolymerization protocols with monoamine, we introduce a catalyst of scandium triflate ($Sc(OTf)_3$) to accelerate the transimination process,[24] shortening depolymerization time by a factor of 8. Leveraging the instability of alkyl-substituted imines, we propose two recovery routes under acidic conditions. The crystallinity, porosity and adsorption capacity of recovered COFs are confirmed by powder X-ray diffraction (PXRD) and physical adsorption measurements.

Results and discussion

Model reactions

Fig. 1b depicts that the transimination direction depends on reaction conditions. We chose an alkyl monoamine of tetrahydrofurfurylamine (THFA), a primary amine featuring a cyclic ether moiety that has strong nucleophilicity with good solubility in either water or organic solvents, to synthesize an alkyl-imine **1** (Reaction I). An aromatic monoamine of 3′,5′-diphenylbiphenyl-4-amine (**2**) was used to produce a compound **3** that contains a typical linkage of imine-linked COFs (Reaction II). Their formation and transimination were studied using MS (Fig. 1c) and liquid chromatography (Fig. S1). In neutral solvents (*e.g.*, methanol and dichloromethane), THFA possessing a stronger nucleophilicity than monomer **2** enabled the transformation of aromatic imine **3** into an alkyl-substituted imine **1** (Reaction III). But in the presence of acetic acid, more basic THFA made itself preferentially protonated, leaving the monomer **2** to revert back to aromatic imine **3** (Reaction IV). Generally, the aromatic imine **3** with a conjugated structure possesses relatively good chemical stability, which is the essential prerequisite for various applications of imine-linked COFs. Our initial proposal was to use an aqueous solution of HCl or NaOH to depolymerize crosslinked COFs, but it was unfeasible (Fig. S2). Based on the amine–imine exchange reaction results, we employed THFA to chemically depolymerize imine-linked COFs.

Room-temperature depolymerization of TAPB-TPA COF

As a demo, TAPB-TPA COF was synthesized through the condensation of 1,3,5-tri(4-aminophenyl)benzene (TAPB) with terephthalaldehyde (TPA) according to our reported method[32] (Fig. 2a, Scheme S1, Fig. S3 and S4, $S_{BET} = 1778\ m^2\ g^{-1}$ and pore width = 2.95 nm). The theoretical content of imine bonds (C=N) was calculated to be 6 mmol per gram of TAPB-TPA COF solid. The depolymerization reaction was carried out at room temperature by mixing THFA and TAPB-TPA COF powder in dichloromethane (Fig. 2a). We set molar ratios of imine bonds to THFA at 1 : 3, 1 : 5 and 1 : 10, respectively, to investigate the depolymerization process. As shown in Fig. 2b, the TAPB-TPA COF dispersed in dichloromethane declined along with the depolymerization time when the 1 : 10 THFA condition was adopted. An obvious change from a turbid yellow suspension to a transparent colloidal dispersion (Fig. S5) was observed. Residual solids in depolymerization mixtures were filtered using a 0.1 μm filter (Fig. 2b, inset, and Fig. S6), weighed, and characterized using a scanning electron microscope (SEM, Fig. S7). Percentages of residual solids regarding to the mass of pristine TAPB-TPA COF were calculated to be 23.0% (1 day), 5.2% (2 days), 3.3% (3 days) and 2.2% (4 days). In contrast, 1 : 3 THFA and 1 : 5 THFA conditions took longer times of 8 and 16 days, respectively, for complete depolymerization (Fig. 2b, S8 and S9). It should be noted that the sharp decline of the TAPB-TPA COF amount occurred within 4 days, corresponding to a residual solid mass of 10.0% for 1 : 3 THFA and 7.0% for 1 : 5 THFA. These results proved that THFA can disassemble imine-linked frameworks of TAPB-TPA COF.

Products in a four-day depolymerization mixture obtained with 1 : 10 THFA were confirmed by MS and NMR techniques. As shown in Fig. 2c, *m*/*z* peaks at 301.1914 and 352.1811 were assigned to a THFA-substituted imine compound (denoted as alkyl-imine) and TAPB monomer, respectively. They were purified through silica flash column chromatography with a mobile phase of petroleum ether/methanol (PE/MeOH, 3 : 1, v/v). Two chromatographic bands of B1 and B2 were observed and assigned to

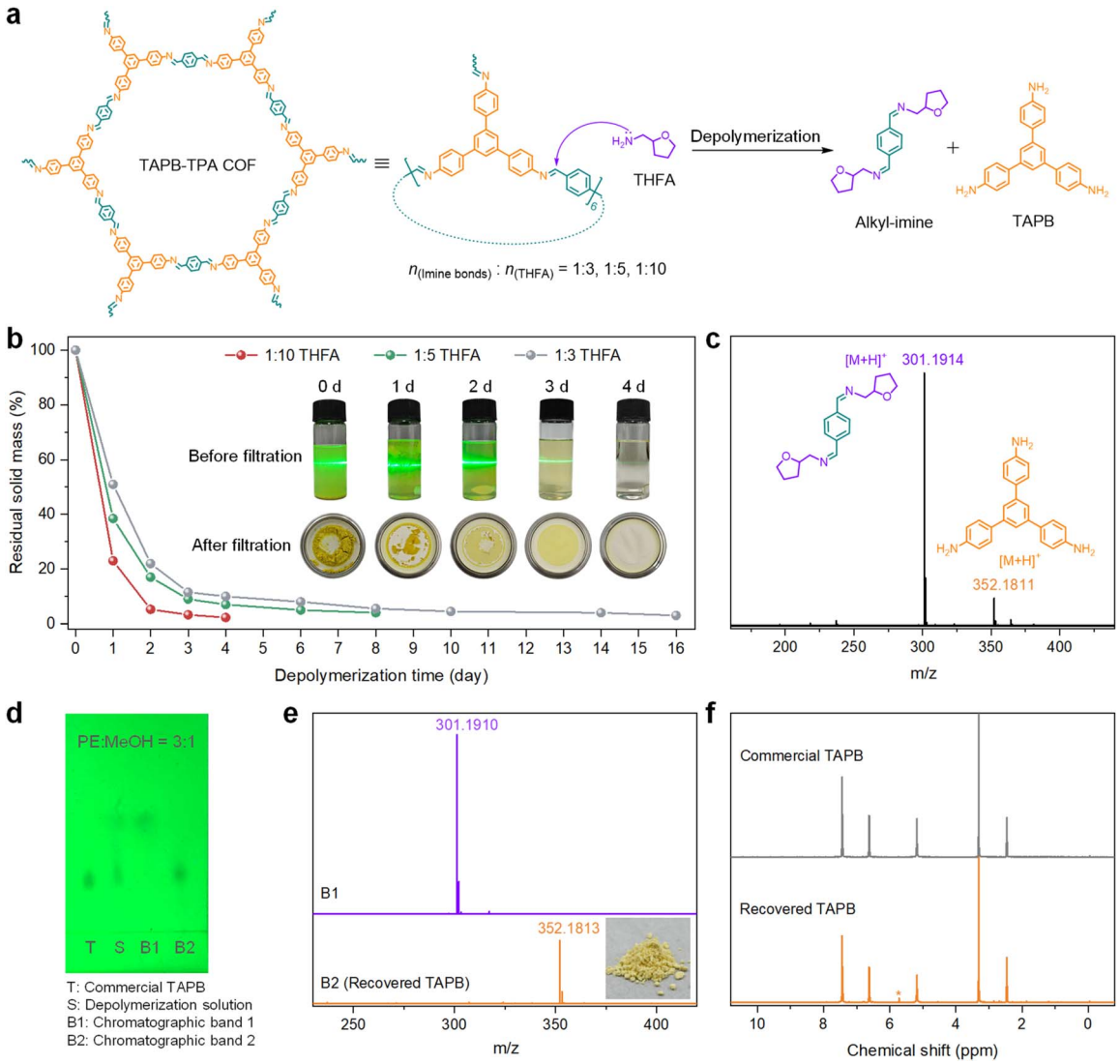

Fig. 2 (a) Schematic illustration for COF depolymerization through dynamic imine chemistry. (b) Depolymerization time-dependent residual solid mass at different ratios of imine bonds to THFA. Inset: photographs of 1 : 10 THFA depolymerization mixtures and residual solids. (c) Mass spectrum of 1 : 10 THFA depolymerization solution (raw data, see also Fig. S64). (d) Thin-layer chromatogram of the commercial TAPB monomer (T), depolymerization solution (S) and products corresponding to column chromatographic bands 1 and 2 (B1 and B2). (e) Mass spectra of purified products (raw data, see also Fig. S65 and S66). Inset: recovered TAPB powder. (f) Comparison of ^{1}H NMR spectra between commercial and recovered TAPB.

alkyl-imine and TAPB monomer as evidenced in the thin-layer chromatogram (Fig. 2d), MS spectra (Fig. 2e) and ^{1}H NMR spectra (Fig. 2f). With respect to the mass of pristine TAPB-TPA COF, 46% TAPB was recovered. We utilized the recovered TAPB and commercial TPA monomer to synthesize a fresh TAPB-TPA COF. Its diffraction peaks at 2.48°, 4.56°, 5.25°, 7.15° and 9.54° were in accordance with the pristine material (Fig. S10). The nitrogen adsorption isotherm indicated a Brunauer–Emmett–Teller (BET) surface area of 1178 $m^2\ g^{-1}$ and characteristic pore width of 2.95 nm for the fresh TAPB-TPA COF (Fig. S11).

Two *in situ* recycling routes for TAPB-TPA COF

Inspired by the transamination reversibility in acetic acid solution (Fig. 1b), we proposed two *in situ* recycling methods for TAPB-TPA COF, including room-temperature recycling (RTR, Route I, Fig. 3a) and solvothermal recycling (STR, Route II, Fig. 3b). Both recycling routes did not require tedious monomer purifications. The depolymerization products underwent an *in situ* reversion back to the crosslinked TAPB-TPA COF (Fig. 3c). As a demonstration, we scaled up the depolymerization mixture by dispersing 200 mg of TAPB-TPA COF in 100 mL of THFA-containing dichloromethane solution. For Route I, aqueous acetic acid (18 mL, 6 mol L^{-1}) was added to the 1 : 10 THFA depolymerization mixture, accompanied by the precipitation of 58% solid (with respect to the theoretical solid mass) at 5 min and an approximate plateau within 40 min (Fig. 3d). In order to achieve the crystalline TAPB-TPA COF, reaction mixtures were stirred at ambient pressure and temperature for 24 h. Route II was built on the success of using the solvothermal method for synthesizing TAPB-TPA COF. Briefly, the depolymerization

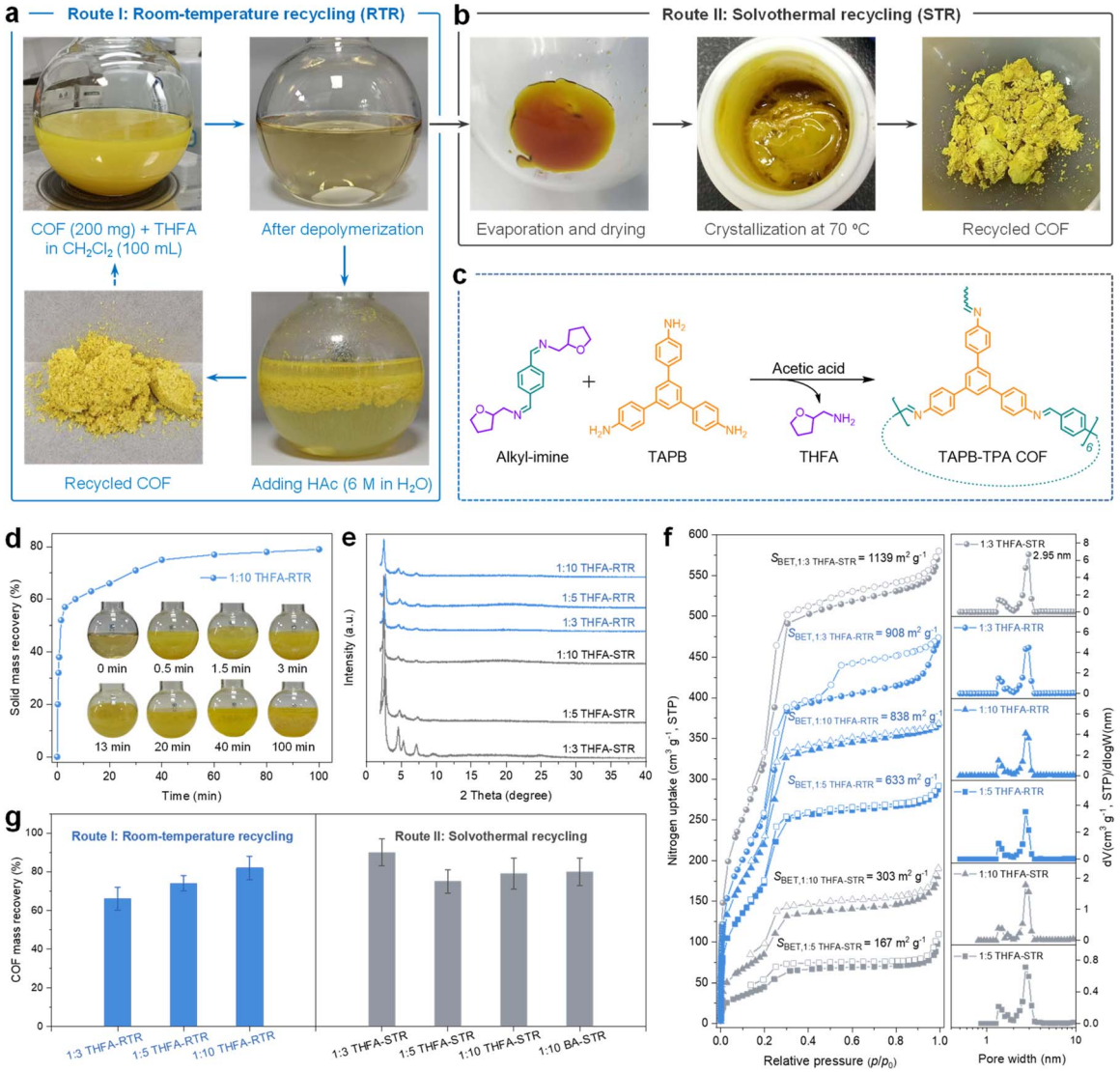

Fig. 3 Schematic illustrations for (a) room-temperature recycling route and (b) solvothermal recycling route. (c) Acetic acid-catalyzed transamination for the TAPB-TPA COF recycling. (d) Solid mass recovery upon addition of acetic acid into the 1 : 10 THFA depolymerization mixture (Route I). Inset: recycling mixture photographs at different times. (e) PXRD patterns of recycled TAPB-TPA COFs. (f) Nitrogen adsorption/desorption isotherms and pore width distributions of recycled TAPB-TPA COFs. (g) Comparison of COF recoveries between Routes I and II. Error bars represent standard deviations of the means of triplicate recycling.

mixtures were evaporated and dried, to which solvents of 1,4-dioxane, 1,3,5-trimethylbenzene, glacial acetic acid and water were added. The resulting mixture was transferred to a Teflon-sealed autoclave and treated at 70 °C for 24 h, regenerating crystalline TAPB-TPA COF (Fig. S12). In the following discussion, TAPB-TPA COFs recycled using different conditions were named 1 : 3, 1 : 5, 1 : 10 THFA-RTR (Route I) and THFA-STR (Route II), respectively.

We examined crystallinities, porosities and mass recoveries of the recycled TAPB-TPA COFs. PXRD patterns indicated that all recycled COFs had typical diffraction peaks (Fig. 3e), in accordance with the pristine TAPB-TPA COF (Fig. S3). Nitrogen adsorption isotherms confirmed that the amount of THFA used at the depolymerization stage affected BET surface areas of recycled COFs, but their pore width was united at 2.95 nm (Fig. 3f). For instance, TAPB-TPA COFs recycled from 1 : 3 THFA depolymerization mixtures showed the highest surface areas of 908 $m^2\ g^{-1}$ (1 : 3 THFA-RTR) and 1139 $m^2\ g^{-1}$ (1 : 3 THFA-STR). The 1 : 10 THFA depolymerization condition, which took the least depolymerization time (4 days), in tandem with two recycling routes, generated surface areas of 838 $m^2\ g^{-1}$ (1 : 10 THFA-RTR) and 303 $m^2\ g^{-1}$ (1 : 10 THFA-STR). The TAPB-TPA COF mass recoveries ranged from 66% to 90% (Fig. 3g), which were higher than the TAPB monomer recovery (46%). Besides THFA, we proved that another alkylamine, *n*-butylamine (BA), can depolymerize TAPB-TPA COF in dichloromethane when the molar ratio of imine bonds to BA was 1 : 10 (Fig. S12). Using Route II, 80% crystalline TAPB-TPA COF was recycled (1 : 10 BA-STR, Fig. 3g and S13), which possessed a BET surface area of 442 $m^2\ g^{-1}$ and pore width of 2.95 nm (Fig. S14). Similar

compositions and morphologies of all recycled TAPB-TPA COFs were confirmed using FT-IR spectra (Fig. S15) and SEM images (Fig. S16), respectively.

Considering that the recycled TAPB-TPA COF showed superior porosity with BA compared to THFA (442 *vs.* 303 $m^2 g^{-1}$), we further tested BA under the optimized THFA recycling conditions (imine/amine = 1 : 3, STR method, Fig. S12). A highly crystalline TAPB-TPA COF with a BET surface area of 735 $m^2 g^{-1}$ was successfully obtained (Fig. S17 and S18), but, unfortunately, its surface area was lower than that obtained using THFA under identical conditions (1139 $m^2 g^{-1}$, Fig. 3f). The difference in BET surface areas among the recycled and pristine COFs was likely attributed to the loss of crystallinity, as evidenced by the full width at half maximum (FWHM) of the (100) diffraction peak (Table S1). Besides, the residual monoamines in depolymerization mixtures might interfere with framework reconstruction, introducing structural defects and increasing the likelihood of pore collapse during drying.

Depolymerization method generality

After developing the depolymerization method for TAPB-TPA COF, we further examined its generality for the structurally diverse COFs, including TFB-N_2H_4 COF (Scheme S2 and Fig. S19–S21), ETTA-TPA COF (Scheme S3 and Fig. S22–S24), COF-LZU1 (Scheme S4 and Fig. S25–S27), COF-300 (Scheme S5 and Fig. S28–S30), $[HC{\equiv}C]_{0.17}$-TAPB-DMTA COF (Scheme S6 and Fig. S31–S33), TAPB-TT COF (Scheme S7 and Fig. S34–S36) and ETTA-TT COF (Scheme S8 and Fig. S37–S39). These frameworks vary in imine linkages and topologies, and some of them contain heteroatom-based functional groups or building blocks with side chains. Their depolymerization kinetics curves are plotted in Fig. 4. As expected, THFA cannot depolymerize TFB-N_2H_4 COF due to its weaker nucleophilicity than hydrazine. A highly efficient depolymerization process was observed for ETTA-TPA COF, $[HC{\equiv}C]_{0.17}$-TAPB-DMTA COF and COF-LZU1. COF-300 having N-fold interpenetrated structures required relatively long time for complete depolymerization. For TAPB-TT COF and ETTA-TT COF, the electron-rich thiophene unit likely reduced the electrophilicity of carbon in imine bonds, resulting in a slow depolymerization rate.

To validate the feasibility of our chemical recycling method across structurally diverse COFs, we selected the $[HC{\equiv}C]_{0.17}$-TAPB-DMTA COF as an example for recovery study. Under the 1 : 10 THFA-RTR condition (Fig. S40), 73% of the crystalline COF was successfully recycled (Fig. S41). The recycled COF possessed a BET surface area of 722 $m^2 g^{-1}$ and pore width of 2.73 nm (Fig. S42), which notably exceeded the value of the pristine $[HC{\equiv}C]_{0.17}$-TAPB-DMTA COF (215 $m^2 g^{-1}$, Fig. S32).

Using $Sc(OTf)_3$ to accelerate the depolymerization process

Despite our depolymerization method demonstrating a good versatility for imine-linked COFs, its practical application is hampered by the trade-off between the depolymerization rate and THFA consumption (Fig. 2a). Based on the abovementioned results, we introduced $Sc(OTf)_3$, a catalyst for the fast amine–imine exchange reaction,[24] to accelerate the depolymerization rates. Fig. 5a shows that the residual solids were calculated to be 12.0% (6 h), 7.0% (18 h), 5.5% (36 h) and 5.0% (48 h) when 4% $Sc(OTf)_3$, with respect to the molar amount of THFA, was adopted in the 1 : 3 THFA depolymerization mixture. The depolymerization time was shortened by a factor of 8 compared to the 16 days required in the absence of the catalyst (Fig. S43). Even though the $Sc(OTf)_3$ amount decreased to 0.5% under the 1 : 3 THFA condition, complete depolymerization can be achieved within 96 h (Fig. S44). This efficiency was comparable to that of the 1 : 10 THFA condition without the use of the catalyst. To make the discussion clearer, the depolymerization conditions are denoted as 1 : *x* THFA-*y*% Sc^{III}, where 1 : *x* indicates the molar ratio of THFA to imine bonds in TAPB-TPA COF and *y* is the molar percentage of $Sc(OTf)_3$ relative to THFA. With 4% Sc^{III}, the TAPB-TPA COF was largely depolymerized within 48 hours even at lower imines/THFA ratios (1 : 2, 1 : 1.5 and 1 : 1), with a depolymerization efficiency of 94.0%, 89.7% and 73.2%, respectively (Fig. 5b and S45).

As depicted in Fig. 6a, the proposed catalyzed transamination mechanism involves the simultaneous coordination of the Sc^{III} center to the nitrogen atoms of both the imine bond and THFA. A key ternary intermediate polarized the imine and facilitated the nucleophilic attack of THFA. Then the resulting gem-diamino intermediate collapsed, completing the amine–imine exchange. The subsequent dissociation of $Sc(OTf)_3$ from the new alkyl-imine enables its regeneration, simultaneously releasing the TAPB monomer. To confirm the Sc^{III}–N coordination, X-ray photoelectron spectroscopy (XPS) analysis was performed (Fig. S46). The residual solid sample was collected using a 0.1 μm filter from the 1 : 3 THFA-4% Sc^{III} depolymerization mixture, followed by washing with water to remove uncombined $Sc(OTf)_3$. This sample, likely representing a Sc^{III}–N coordinated complex, was compared with the pristine TAPB-

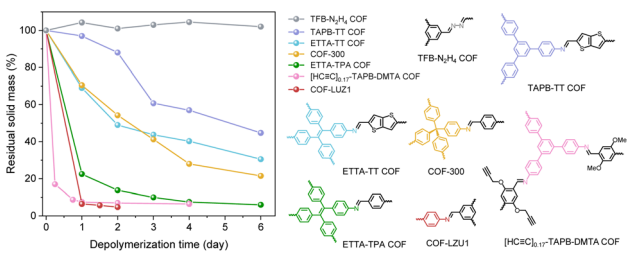

Fig. 4 Depolymerization kinetics under the 1 : 10 THFA condition for COFs with different imine linkages and topologies.

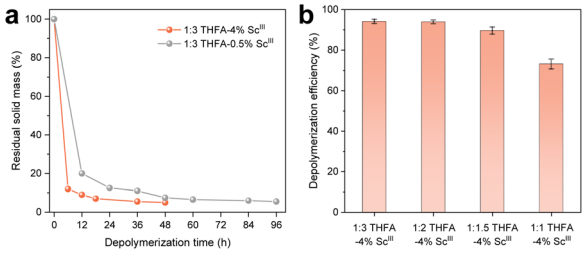

Fig. 5 (a) Depolymerization time-dependent residual solid mass under 1 : 3 THFA in the presence of $Sc(OTf)_3$ to THFA. (b) Effect of THFA amount on depolymerization efficiency.

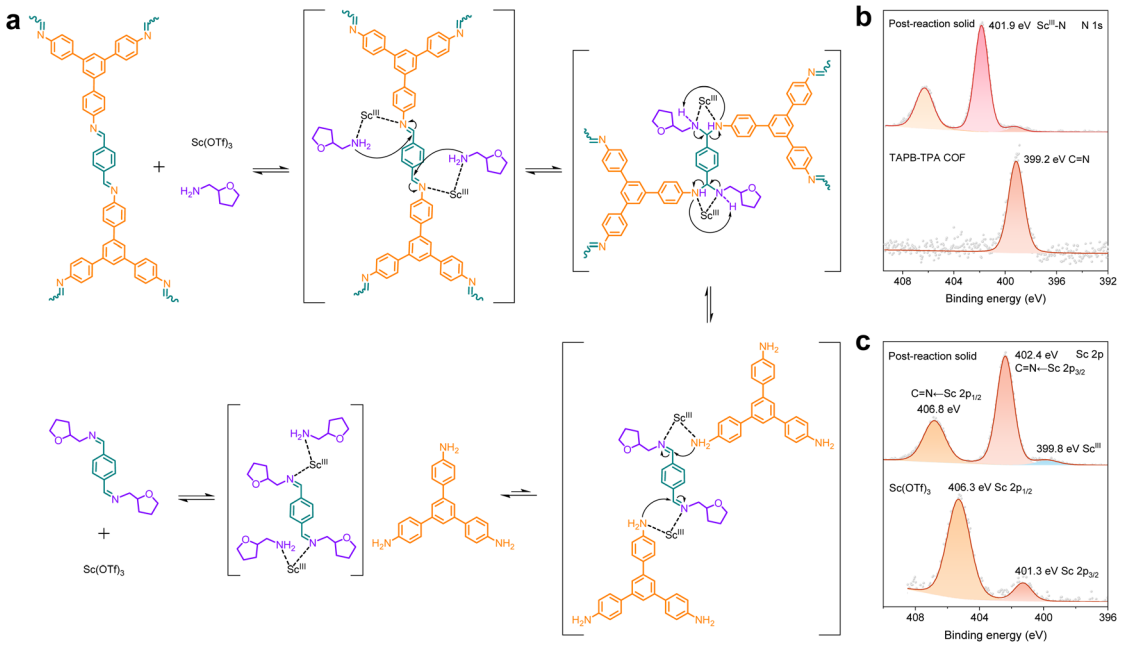

Fig. 6 (a) Schematic illustration for the $Sc(OTf)_3$-catalyzed transamination mechanism. (b) High-resolution XPS N 1s spectra of TAPB-TPA COF and the post-reaction solid. (c) High-resolution XPS Sc 2p spectra of $Sc(OTf)_3$ and the post-reaction solid.

TPA COF and pure $Sc(OTf)_3$. As evidenced in N 1s spectra (Fig. 6b), the characteristic imine peak at 399.2 eV shifted to a higher binding energy of 401.9 eV, indicating a significant loss of electron density on nitrogen atoms. This shift was attributed to the formation of the Sc^{III}–N coordinated complex, which was also confirmed using Sc 2p spectra (Fig. 6c).

We found that excessive amounts of $Sc(OTf)_3$ adversely affected the subsequent reconstruction of COFs (Fig. S47–S49). For instance, using the room-temperature recycling route, we recovered crystalline TAPB-TPA COF from the 1 : 3 THFA-4% Sc^{III} depolymerization products. The TAPB-TPA COF recovered from filtrates showed high crystallinity and BET surface area. Therefore, a filtration step was performed to remove excess $Sc(OTf)_3$ in depolymerization prior to the *in situ* recycling. To identify the optimal balance between the COF and THFA-$Sc(OTf)_3$ amounts, we recorded the room-temperature depolymerization and reconstruction processes in Fig. S50 and summarized recoveries, structural integrities and porosities of recovered TAPB-TPA COF materials. For all depolymerization conditions in tandem with the RTR route, mass recoveries ranged from 79% to 92% (Fig. S51). PXRD patterns confirmed that all recycled COFs displayed typical diffraction peaks. The COFs obtained from 4% $Sc(OTf)_3$ depolymerization mixtures showed stronger intensity peaks compared to 0.5% $Sc(OTf)_3$ counterparts (Fig. S52). Nitrogen adsorption isotherms revealed their pore widths at 2.73 nm and 2.95 nm (Fig. S53). The recovered TAPB-TPA COF using the 1 : 3 THFA-4% Sc^{III} condition exhibited the highest specific surface area of 709 $m^2\ g^{-1}$, while the 1 : 3 THFA-0.5% Sc^{III} condition in tandem with the RTR route generated only a surface area of 145 $m^2\ g^{-1}$.

To further evaluate the potential application of our recycling strategy for end-of-life COFs, the pristine TAPB-TPA COF was intentionally damaged by stirring in 1 mol L^{-1} HCl for 12 h. The treated COF showed severe losses of crystallinity (Fig. S54) and BET surface area, from 1778 $m^2\ g^{-1}$ to 167 $m^2\ g^{-1}$ (Fig. S55). As evidenced in Fig. S56 and S57, the end-of-life TAPB-TPA COF was successfully restored using our recycling method of 1 : 3 THFA-4% Sc^{III}-RTR, whose BET surface area increased from 167 $m^2\ g^{-1}$ to 747 $m^2\ g^{-1}$. The mass recovery was calculated to be 88%.

Comparison of depolymerization and recycling routes

The depolymerization conditions and recycling methods (*e.g.*, processing time, mass recovery, crystallization, and BET surface area) are summarized in Tables S2 and S3. Without the use of $Sc(OTf)_3$, the 1 : 10 THFA depolymerization condition (4 days) in tandem with the room-temperature recycling route (1.5 days) is time-saving, regenerating the TAPB-TPA COF with a comparable surface area. The 1 : 3 THFA condition consumed fewer reagents, but took more time, 16 days, for complete depolymerization. If we can accept the compromise of 90% depolymerization within 4 days, either using 1 : 3 THFA-RTR or 1 : 3 THFA-STR as an alternative strategy is recommended for the recycling of high-quality TAPB-TPA COF. In contrast, the introduction of $Sc(OTf)_3$ remarkably accelerated depolymerization rates. This allows for not only shortening depolymerization time from 16 to 2 days (1 : 3 THFA-4% Sc^{III}), but also efficient depolymerization even at lower THFA/COF ratios. Additionally, we plotted BET surface areas *versus* depolymerization time in Fig. S58. Among the evaluated conditions, 1 : 3 THFA-4% Sc^{III}-RTR is recommended as the optimal strategy for recycling high-quality TAPB-TPA COF.

We found that it was difficult to reconstruct crystallinity and porosity as good as those of the pristine TAPB-TPA COF. As we know, the preparation of COFs is very sensitive to the synthesis conditions (*e.g.*, solvents, catalyst, temperature, and time). Unlike synthesizing COFs starting with pure monomers,

residual THFA, catalyst and solvents in the depolymerization mixtures would affect their reconstructions. As such, two recycling routes depicted in Fig. 3a and b were built on a number of attempts.

To functionally assess the pore accessibility of the recycled COFs, we performed benzene vapor adsorption measurements. Benzene has attracted much attention among volatile organic compounds due to its high toxicity. Our previous study has shown the potential application of COFs for benzene removal.[4] Here, we utilized benzene as a probe to give an insight into changes in available pores and adsorption capacity between pristine and recycled TAPB-TPA COFs. Consequently, due to the difference in BET surface area between recovered and pristine TAPB-TPA COFs, the benzene vapor adsorption decreased from 14.68 to 5.94 mol per gram of COF (Fig. S59).

Conclusions

In conclusion, we have demonstrated chemical recycling methods of TAPB-TPA COF through dynamic imine chemistry. As evidenced in this work, alkyl monoamines can attack the aromatic imine linkages of COFs in neutral organic solvents, depolymerizing the crosslinked frameworks into small molecules. Moreover, it was found that the combination of monoamines with $Sc(OTf)_3$ remarkably accelerates the depolymerization process, offering a time-saving protocol. Without tedious monomer purifications, we have realized the *in situ* regeneration of crystalline COFs in complex depolymerization mixtures. Given that most imine-linked COFs are made using aromatic amine building blocks, we anticipate that these findings on their closed-loop recycling open up an avenue in the sustainable development of porous organic materials. Last but not least, we have proved the versatility of a monoamine–imine exchange-based depolymerization strategy for aromatic imine-linked COFs and demonstrated a case study for the reconstruction of TAPB-TPA COF. But we must honestly point out that the optimal reconstruction conditions vary for each building block and framework. Additionally, for COFs that were synthesized by post-modifications or suffered from imine linkage damage, the chemical recycling method in this work needs to be further studied.

Author contributions

The manuscript was written through contributions of all authors. All authors have given approval to the final version of the manuscript.

Conflicts of interest

There are no conflicts to declare.

Data availability

The data supporting this article have been included as part of the supplementary information (SI). Supplementary information is available. See DOI: https://doi.org/10.1039/d5sc09502f.

Acknowledgements

This study was supported by grants from the National Natural Science Foundation of China (22372097 to Z. Liu; 22132002 to Y. Fang) and the Fundamental Research Funds for the Central Universities (GK202302001).

References

1 Y. Liu, X. Liu, A. Su, C. Gong, S. Chen, L. Xia, C. Zhang, X. Tao, Y. Li, Y. Li, T. Sun, M. Bu, W. Shao, J. Zhao, X. Li, Y. Peng, P. Guo, Y. Han and Y. Zhu, *Chem. Soc. Rev.*, 2024, **53**, 502–544.
2 X. Liu, H. Pang, X. Liu, Q. Li, N. Zhang, L. Mao, M. Qiu, B. Hu, H. Yang and X. Wang, *Innovation*, 2021, **2**, 100076.
3 S. Karak, K. Dey, A. Torris, A. Halder, S. Bera, F. Kanheerampockil and R. Banerjee, *J. Am. Chem. Soc.*, 2019, **141**, 7572–7581.
4 Y. Su, M. Qin, J. Kong, Q. Zhai, D. Yuan, Z. Liu and Y. Fang, *Adv. Funct. Mater.*, 2024, **34**, 2400433.
5 W. Ji, L. Xiao, Y. Ling, C. Ching, M. Matsumoto, R. P. Bisbey, D. E. Helbling and W. R. Dichtel, *J. Am. Chem. Soc.*, 2018, **140**, 12677–12681.
6 R. Wang, Y. Zhou, Y. Zhang, J. Xue, J. Caro and H. Wang, *Adv. Mater.*, 2022, **34**, 2204894.
7 Z. Guo, H. Wu, Y. Chen, S. Zhu, H. Jiang, S. Song, Y. Ren, Y. Wang, X. Liang, G. He, Y. Li and Z. Jiang, *Angew. Chem., Int. Ed.*, 2022, **61**, e202210466.
8 J. Liu, G. Han, D. Zhao, K. Lu, J. Gao and T.-S. Chung, *Sci. Adv.*, 2020, **6**, eabb1110.
9 C. Jin, N. Li, E. Lin, X. Chen, T. Wang, Y. Wang, M. Yang, W. Liu, J. Yu, Z. Zhang and Y. Chen, *ACS Catal.*, 2022, **12**, 8259–8268.
10 C. Krishnaraj, H. Sekhar Jena, L. Bourda, A. Laemont, P. Pachfule, J. Roeser, C. V. Chandran, S. Borgmans, S. M. J. Rogge, K. Leus, C. V. Stevens, J. A. Martens, V. Van Speybroeck, E. Breynaert, A. Thomas and P. Van Der Voort, *J. Am. Chem. Soc.*, 2020, **142**, 20107–20116.
11 H. S. Sasmal, S. Bag, B. Chandra, P. Majumder, H. Kuiry, S. Karak, S. Sen Gupta and R. Banerjee, *J. Am. Chem. Soc.*, 2021, **143**, 8426–8436.
12 X. Liu, R. Huang, L. Peng, J. Yang, J. Yan, B. Zhai, Y. Luo, C. Zhang, S. Tan, X. Liu, L. Ding and Y. Fang, *Angew. Chem., Int. Ed.*, 2025, **64**, e202414472.
13 G. Das, B. P. Biswal, S. Kandambeth, V. Venkatesh, G. Kaur, M. Addicoat, T. Heine, S. Verma and R. Banerjee, *Chem. Sci.*, 2015, **6**, 3931–3939.
14 A. Jrad, G. Das, N. Alkhatib, T. Prakasam, F. Benyettou, S. Varghese, F. Gándara, M. Olson, S. Kirmizialtin and A. Trabolsi, *Nat. Commun.*, 2024, **15**, 10490.
15 Z. Li, N. Huang, K. H. Lee, Y. Feng, S. Tao, Q. Jiang, Y. Nagao, S. Irle and D. Jiang, *J. Am. Chem. Soc.*, 2018, **140**, 12374–12377.
16 Z. T. Kralles, P. K. Deherikar, C. A. Werner, X. Hu, E. P. Kolodziej and N. Dai, *Environ. Sci. Technol.*, 2024, **58**, 17497–17509.

17 Q. Sun, B. Aguila, L. D. Earl, C. W. Abney, L. Wojtas, P. K. Thallapally and S. Ma, *Adv. Mater.*, 2018, **30**, 1705479.
18 S. He, T. Zeng, S. Wang, H. Niu and Y. Cai, *ACS Appl. Mater. Interfaces*, 2017, **9**, 2959–2965.
19 L. Zhu, L. Ding, J. Kong, Y. Fang and Z. Liu, *Cell Rep. Phys. Sci.*, 2025, **6**, 102813.
20 M. E. Belowich and J. F. Stoddart, *Chem. Soc. Rev.*, 2012, **41**, 2003–2024.
21 G. Melchiorre, L. Visieri, M. Valentini, R. Cacciapaglia, A. Casnati, L. Baldini, J. A. Berrocal and S. Di Stefano, *J. Am. Chem. Soc.*, 2025, **147**, 11327–11335.
22 M. Ciaccia and S. Di Stefano, *Org. Biomol. Chem.*, 2015, **13**, 646–654.
23 M. Ciaccia, R. Cacciapaglia, P. Mencarelli, L. Mandolini and S. Di Stefano, *Chem. Sci.*, 2013, **4**, 2253–2261.
24 N. Giuseppone, J.-L. Schmitt, E. Schwartz and J.-M. Lehn, *J. Am. Chem. Soc.*, 2005, **127**, 5528–5539.
25 J. Wang, R. Wen, J. Kong, J. Liu, Z. Liu and Y. Fang, *Angew. Chem., Int. Ed.*, 2025, **64**, e202502020.
26 F. J. Uribe-Romo, J. R. Hunt, H. Furukawa, C. Klöck, M. O'Keeffe and O. M. Yaghi, *J. Am. Chem. Soc.*, 2009, **131**, 4570–4571.
27 T. Ma, E. A. Kapustin, S. X. Yin, L. Liang, Z. Zhou, J. Niu, L.-H. Li, Y. Wang, J. Su, J. Li, X. Wang, W. D. Wang, W. Wang, J. Sun and O. M. Yaghi, *Science*, 2018, **361**, 48–52.
28 J. Han, J. Feng, J. Kang, J.-M. Chen, X.-Y. Du, S.-Y. Ding, L. Liang and W. Wang, *Science*, 2024, **383**, 1014–1019.
29 M. Ciaccia, S. Pilati, R. Cacciapaglia, L. Mandolini and S. Di Stefano, *Org. Biomol. Chem.*, 2014, **12**, 3282–3287.
30 Y. Zhang, S. Xie, M. Yan and O. Ramström, *Chem.–Eur. J.*, 2017, **23**, 11908–11912.
31 D. Schultz and J. R. Nitschke, *J. Am. Chem. Soc.*, 2006, **128**, 9887–9892.
32 L. Zhu, Y. Su, Z. Liu and Y. Fang, *Small*, 2023, **19**, 2205501.